Journal of Mines and Geosciences
ISSN 3057-3483

# Spatial distribution of petroleum system elements in the Pangani rift basin of north-eastern Tanzania based on interpretation of gravity and magnetic datasets

Ernest Selestin[1,*], Emily Barnabas Kiswaka[1], Obeid Saitabau Lemna[2], Elisante Elisaimon Mshiu[2]

[1]Department of Petroleum Science and Engineering, P.O. Box 35052, University of Dar es Salaam, Tanzania,

[2]Department of Geosciences, P.O. Box 35052, University of Dar es Salaam, Tanzania

*Corresponding author: ernestmziray24@gmail.com

**Keywords**

Pangani rift basin, potential field data, igneous intrusions, volcanic, petroleum potential

**Article information**

*Submit: 13th February. 2024*

*Reviewed: 15th August 2024*

*Accepted: 3rd Nov 2024*

*Publ: 21st Nov 2024*

**Abstract**

There are limited studies on the occurrence and spatial distribution of petroleum system elements in the Pangani Rift Basin (PRB) of northeastern Tanzania. The elements include magmatic intrusions, sediment thickness, and faults and fold structures. This study aimed at assessing the petroleum potential of the PRB based on distributions of these elements. To meet the focus of this work, interpretation of gravity and magnetic datasets was employed. Results show that the basin contains thin and thick sedimentary covers ranging from 0.25 to 2.5 km, respectively. Thick sedimentary successions are found in the northern and southern parts of the basin; the central part contains thin sedimentary cover. Overall, sedimentary fills are thickening westward, toward the NNW-SSE trending master fault. Other mapped major faults have the N-S and NNE-SSW trends. Results of magnetic data interpretation also show that igneous intrusions are present in the PRB and they have produced several fold structures; are dominantly increasing toward the northern part of the basin. The locations of these intrusions conform to locations of different faults suggesting tectonic influence in magmatism. The maximum estimated depth of 2.5 km is favorable for deposition, preservation, and cooking of organic material for possible petroleum generation.

## Introduction

Hydrocarbon resources have been discovered in a variety of geological settings through the interpretation of potential field data i.e. gravity and magnetic data (Dentith & Cowan, 2011). Petroleum is commonly found in sedimentary basins with working petroleum systems. These basins, among others, include East African Rift basins that were formed due to continental rifting (Macgregor, 2015). The rift basins have high geothermal gradient that can facilitate the maturation of source rocks when the right type and quantity of organic matter is present (Monreal et al., 2009). Examples of the East African Rift basins, to mention a few, include the Lokichar (Kenya), Pangani (Tanzania) and Albertine (Uganda) sub-basins. Petroleum accumulations have been discovered in the Albertine and Lokichar basins (Witte et al., 2016). These basins have similar characteristics in terms of geology, geochemistry, and tectonics with basins found in Tanzania. This work is aiming at interpreting potential field datasets in the Pangani rift basin (PRB) of the northeastern Tanzania to assess possible presence and distribution of key petroleum system elements. The interpretation of gravity and magnetic datasets aid assessment of hydrocarbon potential of the basin through establishment of sediment thickness and distribution of key elements that may facilitate source rock maturation, petroleum generation, migration and trapping.

Previous studies focused on identification of lithologies, establishment of lithostratigraphy and improved

understanding of tectonic settings of the PRB (McConnell, 1972; Mbede, 2001; Baker, 2012). None of these workers focused on depositional and post-depositional architectural elements required to understand the petroleum potential of the PRB. These elements, among others, include sediment thickness and spatial distribution of igneous intrusions and other structural features (such as folds and faults); may be established based on qualitative and quantitative interpretation of magnetic and gravity datasets, the approaches that were employed to accomplish this work. Interpretation of the potential field data in the PRB was done by using Oasis Montaj software (e.g., Blaikie et al., 2014; Lemna et al., 2019). The qualitative interpretation focused on the observation and identification of faults, folds/structural highs, and igneous intrusions while the quantitative interpretation allowed the estimation of sediment thickness, size and location of the bodies that are causing the observed anomalies (Thompson, 1982; Reid et al., 1990).

**Tectonic Settings and Basin Development**

The PRB forms the eastern arm of the eastern branch of the East African Rift System (EARS) (Mbede, 2001; Fig. 1a). The EARS began during the Cenozoic due to mantle upwelling and has been active to recent times (Franke et al., 2015). The mantle upwelling caused extension, thinning and opening of the crust (Chorowicz, 2005). The EARS propagate from the Afar region toward Zambezi River, with the approximated length of about 6000 km (Chorowicz, 2005; Ferdinand, 2021). The southward propagation of the EARS caused lithospheric subdivision forming three main rift compartments named the Main Ethiopian Rift (MER), Western branch (WB) and Eastern branch (EB) (Ring, 2014). The MER and WB are not the focus of this study, instead the PRB which forms the eastern arm of the EB was studied. The EB (Fig. 1a) extends for about 2200 km from the Afar triple junction in the north, through the Main Ethiopian Rift, then Northern Kenya toward the Northern part of Tanzanian Divergent where divides itself into three segments/arms (Ebinger et al., 1997; Foster et al., 1997; Mbede, 2001; Chorowicz, 2005; Le Gall et al., 2008). These segments/arms are the Eyasi-Wembere (NE-SW trending), Natron-Manyara-Balangida (N-S trending), and Pangani (NNW-SSE trending) rift arms (Mbede, 2001; Ring, 2014; Fig. 1a).

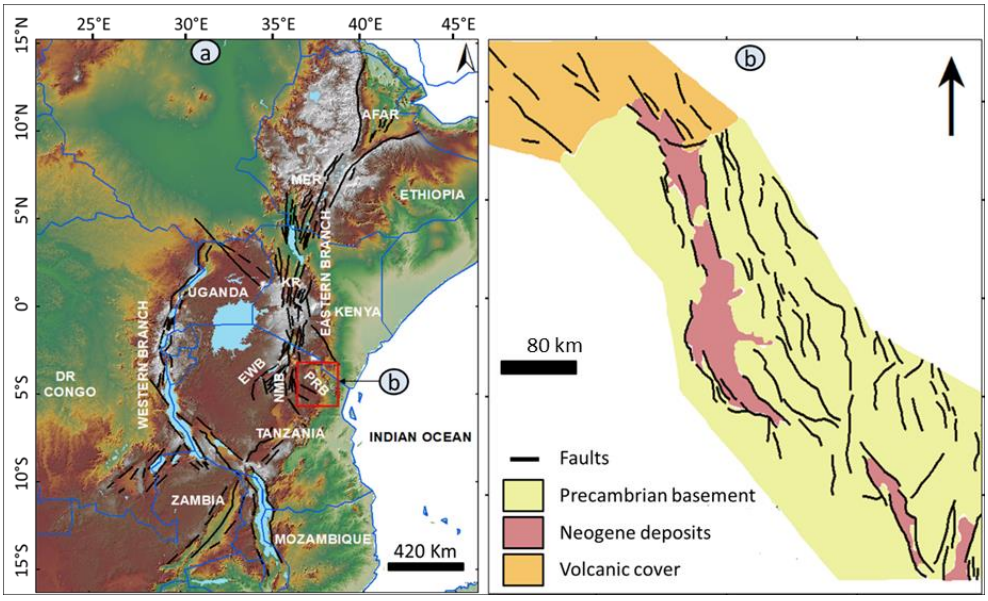


**Figure 1: a)** Shuttle Radar Topography Mission (SRTM) Digital Elevation Model (DEM) showing locations of different components of the EARS (modified from Ring (2014) and Lemna et al. (2019)). EWB= Eyasi-Wembere Basin,

NMB= Natron-Manyara-Balangida Basin, PRB= Pangani Rift Basin, and MER= Main Ethiopian Rift. **b**) Geological and structural elements map of the PRB showing basin trend and distribution of faults and main lithologies in the study area (modified from Baker (2012)).

Development of the EARS is linked to widespread volcanic eruptions that caused deposition of volcaniclastic successions and emplacement of igneous intrusions in the PRB during the Miocene, Plio-Pleistocene and Pliocene-Holocene periods (Bagdasaryan et al., 1973; Mbede, 2001; Mollel & Swisher III, 2012). These volcanic eruptions caused emplacement of igneous bodies and volcanic products with varying composition (Chorowicz, 2005). Magmatic activities and volcanism have direct impact to the petroleum potential of different sedimentary basins as far as source rock maturation, reservoir modification and trap formation are taken into consideration (Planke et al., 2005). This is why the current work is partly aiming at assessing the distribution of igneous intrusions in the PRB.

**Geology and Stratigraphy**

The PRB is a narrow and elongated (NNW-SSE trending) basin surrounded and floored by the Proterozoic metamorphic basement rocks belonging to the Mozambique Belt (Mbede, 2001; Baker, 2012; Fig. 1b). The basin contains well-developed Neogene clastic and volcaniclastic successions (Fig. 1b). Relatively extensive volcanic cover occurs in the north and western extents of the PRB (Baker, 2012; Fig. 1b).

The PRB stratigraphy contains different rock types and its development was due to an interplay of multiple factors including long-lived extensional tectonics and the associated episodic fault reactivations, sediment erosion and transportation, and magmatic activities and volcanism (Mbede, 2001). There is no formal lithostratigraphic scheme that has been established to explain the vertical distribution of rocks in the PRB. The current stratigraphy (Fig. 2) has been updated from Mbede (2001) and Baker (2012). The PRB stratigraphy begins with the Late Proterozoic metamorphic basement rocks (Fig. 2). The basement geology resulted from the amalgamation of cratonic blocks during formation of the Gondwana supercontinent (Macheyeki et al., 2008). The Late Proterozoic metamorphic basement is overlain by debritic and lahah mudflow deposits that are followed by the volcaniclastic successions available in different parts of the basin. This phase of basin development was followed by lacustrine limestone deposition reflecting influence of climate variability in the basin history just before the dominance of clastic sedimentation in the depositional system (Fig. 2). The clastic sedimentation resulted in deposition of clay and sandy successions overlying the lacustrine limestone bodies. During this time period, a volcanic event occurred and caused pyroclastic flow deposition. The pyroclastic deposits are now overlain by the alluvium, red soil and sandy clay (Fig. 2). Deposition of the upper part of the PRB stratigraphy is interpreted to have been influenced by massive volcanism and active fault movements. This is reflected by presence of widely distributed basaltic boulders and fan deposits composed of slope talus, respectively. The slope talus deposits are linked to slope failure attributed to possible tectonic disturbances.

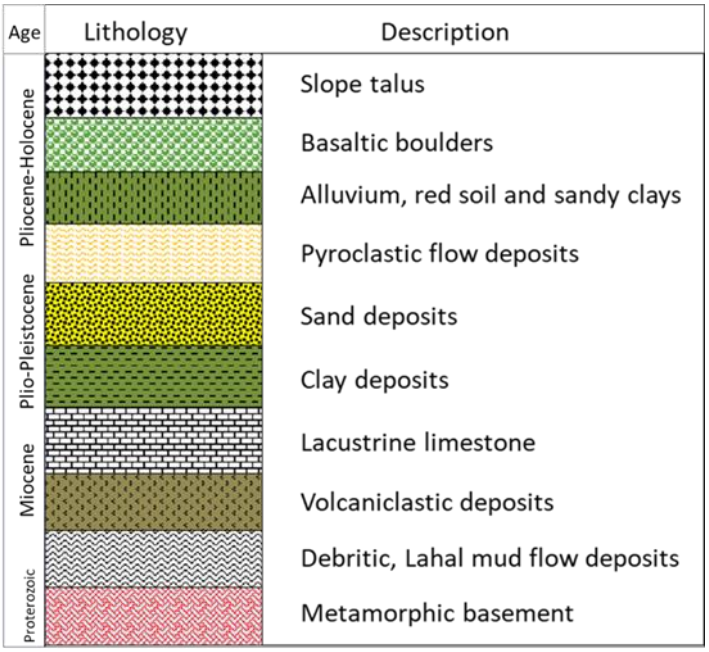


**Figure 2**: Generic lithostratigraphic scheme of the PRB (after Mbede (2001) and Baker (2012)).

**Datasets and Methods**

**Datasets**

This work involved interpretation of potential field (gravity and magnetic) datasets. The available potential field data were acquired by the New Resolution Geophysics (NRG) between July and August 2012. Equipment's that were used to acquire data included Bartington fluxgate magnetometer, Modified GT1A Gravimeter, 2X Scintrex CS3, Novatel 3151R GPS, Rosemount barometer and Free Flight altimeter. Different parameters such as flight altitude, line spacing and traverse line orientation were important during data acquisition. The gravity data was acquired at a flight altitude of 2150 m, line spacing of 2000 m, traverse line orientation of 900, tie line spacing of 8000 m, and tie-line orientation of $0^0$. The magnetic data was acquired at a flight altitude of 100 m above the ground level, line spacing of 2000 m, traverse line orientation of 900, tie line spacing of 8000 m, and tie-line orientation of $0^0$. During and after data acquisition, the NRG did all the corrections to allow data quality enhancement and improved interpretations. The performed corrections include instrumental drift, tides, free-air, Bouguer, and terrain corrections for gravity data, and IGRF correction for magnetic data.

**Methods**

The available datasets (both gravity and magnetic) were analyzed by using Oasis Montaj software that allowed data manipulation and interpretation.

**Gravity Data Transformation**

The gravity data were gridded using a minimum curvature algorithm with a grid cell size of 400 m to produce Bouguer gravity anomaly map (Briggs, 1974; Fig. 3a). Usually, the grid cell size is selected as one-fifth of the line spacing, thus 400 m was optimal for the line spacing of 2000 m through which the current data was acquired. Thereafter, regional and local anomalies were separated from residual anomaly by using Butterworth-filtering technique with a cutoff wavelength of 125 km. The cutoff wavelength of 125 km was selected due to clear variation of color aggregates and density reflecting significant noise reduction.

**Magnetic Data Transformation**

The magnetic data were gridded by using a minimum curvature algorithm with a grid cell size of 400 m as one-

fifth of the line spacing (Briggs, 1974) to produce Total Magnetic Intensity (TMI) map (Fig. 4a). Reduced to pole (RTP) was employed to the TMI map with inclination and declination of -29.89° and - 0.51°, respectively in order to reduce the skewness of the magnetic anomalies and center them over their causative bodies (e.g., Ganiyu et al., 2013). Following this transformation, tilt derivative technique was then applied in order to facilitate delineation of structural elements in the RTP-TMI maps (Verduzco et al., 2014). Finally, Euler deconvolution and spectral depth analysis techniques were used for the estimation of depths and sizes of the magnetic sources.

## Results and Interpretation

### Gravity and Magnetic Results

Gravity and magnetic data analysis and processing allowed production of different anomaly maps reflecting surface and sub-surface geological of the PRB. These maps reflect density and magnetic susceptibility contrasts due to mineralogical and lithological variations (Figs. 3 & 4) that allowed mapping of structural features, determination of basin geometry and trend, and estimation of depth to magnetic basement (sediment thickness) of the study area.

### Gravity Results

Fig. 3 shows Bouguer, regional and residual gravity anomaly maps of the study area. The Bouguer gravity anomaly map (Fig. 3a) shows general density variations in the PRB. These variations are clearly revealed by the separated regional and residual Bouguer gravity anomaly maps (Fig. 3b & c). Gravity anomalies range from -95.6 to -69.7 mGal and from -8.5 to 5.0 mGal for regional and residual Bouguer gravity anomaly maps, respectively. Regional Bouguer gravity anomaly map (Fig. 3b) shows dominance of low Bouguer anomaly in the northern, high Bouguer gravity anomaly in the southern, and medium gravity anomaly in the central parts of the PRB. The northwestern, eastern and southeastern parts of the PRB are characterized by high residual Bouguer gravity anomaly indicative of shallow seated metamorphic basement. It is in these areas where the PRB is flanked by the Kilimanjaro and Meru, Pare and Usambara mountains, respectively (Mbede, 2001; Baker, 2012). However, the north, south and southwestern parts of the PRB are dominated by low residual Bouguer gravity anomalies indicative of thick sedimentary cover. The more or less cone shaped features aligned along the NNW-SSE trending features (Fig. 3c) suggest presence of NNW-SSE trending igneous intrusions in the PRB. The western central and southwestern parts of the area show circular geometry demarcating a low-high Bouguer gravity anomaly. This is probably marking the Masai plateau (Mbede, 2001; Baker, 2012). Generally, the residual Bouguer gravity anomaly map (Fig. 3b) indicates southwest and westward thickening of sediment in the PRB.

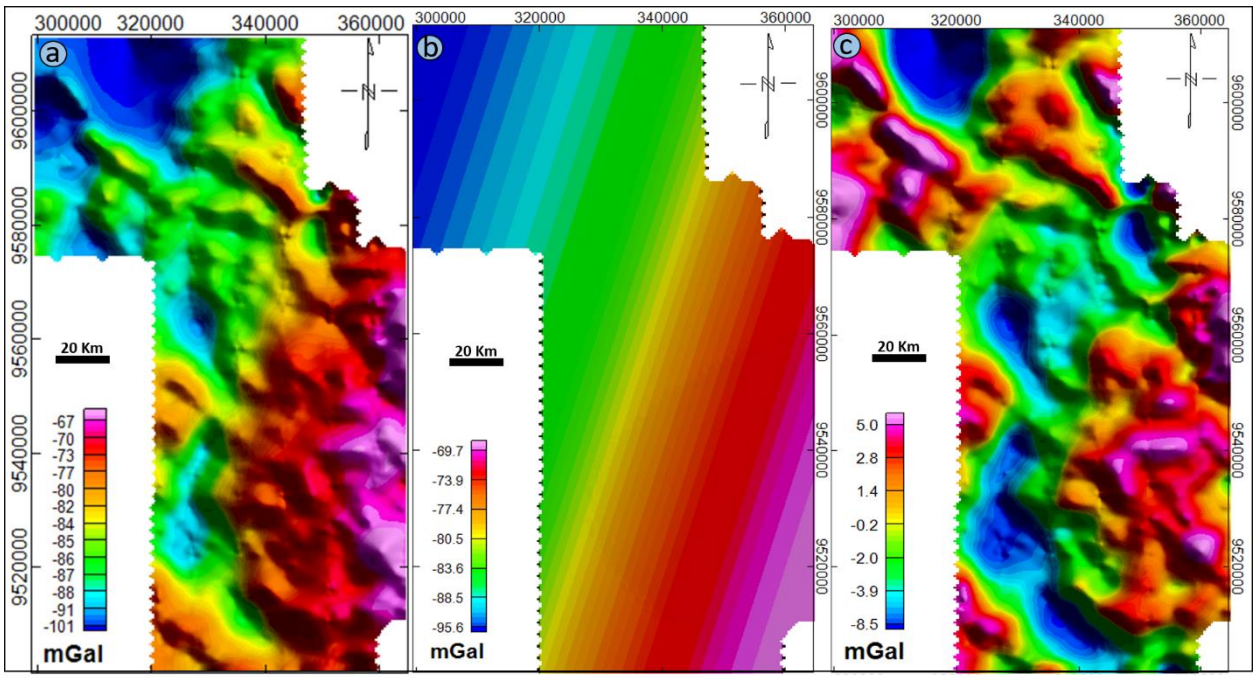


**Figure 3: a)** The Bouguer gravity anomaly b) The Regional Bouguer gravity anomaly and c) Residual Bouguer gravity anomaly maps showing distribution of the gravity anomalies in the PRB.

**Magnetic Results**

The magnetic results are presented based on the generated TMI, RTP-TMI and tilt derivative maps (Figs. 4a, b & c). The TMI and RTP-TMI maps show the ranges of magnetic signatures between -115 to 88 nT and -259 to 136 nT, respectively (Figs. 4a & b). These maps show high magnetic anomalies indicative of shallow metamorphic basement in the northwestern and eastern parts of the PRB. Tilt derivative map shows that low magnetic anomalies dominate the northern part of the basin where NNW-SSE, N-S and NNE-SSW trending lineaments are observed (Fig. 4c). The low magnetic anomalies indicate thick sedimentary cover while the lineaments are the faults dissecting the PRB. The low magnetic anomaly zone at the western center part of the basin (Fig. 4) coincides with the medium to high residual gravity anomaly that has been interpreted to represent the Masai plateau (Fig. 3). Several small-sized oval- and cone-shaped high magnetic anomalies indicative of igneous intrusions occur along the NNW-SSE trending faults and are dominantly increasing toward the north and northwest of the basin (Fig. 4b).

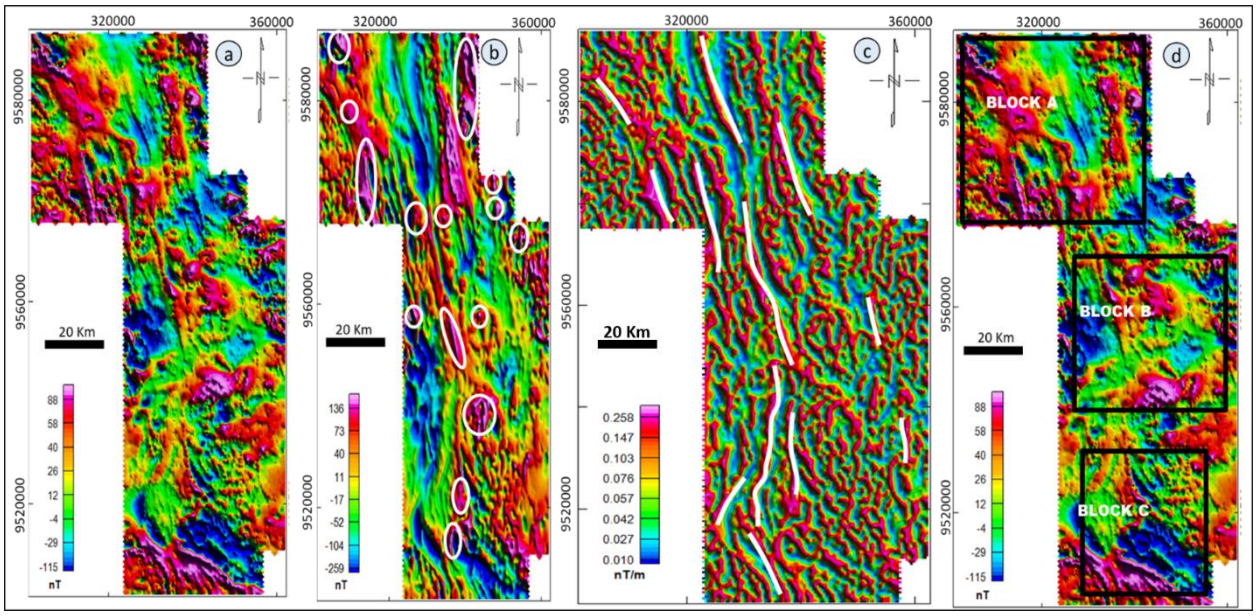


**Figure 4: a**) Total magnetic intensity (TMI) map showing variation of magnetic anomalies in the PRB, b) RTP-TMI map showing several igneous intrusions (white solid lines) characterized by high magnetic signatures, c) Tilt derivative map of the PRB. White lines show locations and trends of the faults dissecting the PRB, and d) Subdivision of the total magnetic intensity map into three major blocks (A, B and C) for the estimation of sediments thickness by using spectral depth analysis.

**Depth Estimation**

This section presents depth estimation results for sedimentary deposits in the PRB. This was done through determination of thickness of sedimentary successions to the causative bodies, their size and corresponding aerial extent. The adopted methods were Euler deconvolution and Spectral depth analysis. The Euler deconvolution technique depends on the geometry of the magnetic sources and structural index, while spectral depth analysis estimates the mean depth in a given area. The estimated mean depth is normally extracted from the produced power spectrum plots that are used to calculate depth for deep and shallow magnetic sources (Telford et al., 1990; Nabighian et al., 2005).

**Located Euler Deconvolution**

The planar view of the revealed igneous bodies and their conformity to the fault systems (Fig. 4b) suggest the dominance of igneous dikes and potential sills which can be modeled by using structural indices of 1 and 2. However, sills and dikes are often linked to deep-seated lopoliths and laccoliths (Corry, 1988). This implies possible presence of deep-seated lopoliths and laccoliths which can be modeled as spheres (SI =3). The SI choice depends on the shape and nature of the modeled igneous body (Uieda et al., 2014). Therefore, the Located Euler deconvolution solutions for structural indices of 1, 2, 3 and 0 (Fig. 5a-d) are given in this section to account for sediment thickness based on depth positions and shapes of different igneous bodies. Many solutions result when 1, 2 and 3 structural indices were used (Fig. 5a-c) while two solutions were obtained when the SI of 0 was used (Fig. 5d). Based on the SI value of 1, the estimated depth to the magnetic source ranges from less than 0.25 to greater than 1.25 km (Fig. 5a). Solutions for the SI value of 1 revealed that sediment cover is relatively thin at the central part of the PRB while thick sedimentary successions are present in the northern and southern parts of the basin (Fig. 5a). The SI value of 2 produced a located Euler deconvolution map showing depth variations ranging

from less than 0.5 to 2.5 km (Fig. 5b). The depth values are relatively small at the central part of the basin (less than 0.5 to 1.5 km), intermediate at the southern part (less than 0.5 to 2 km) and high at the northern part of the basin (less than 0.5 to 2.5 km). The SI value of 3 produced a located Euler deconvolution map showing depth variations ranging from less than 0.5 to 2.5 km (Fig. 5b). Based on the SI of 3, the calculated solutions show low depth values at the central part of the basin (0.5 to 2 km), intermediate at the southern part (0.5 to 2 km) and high at the northern part of the basin (0.5 to 2.5 km). The Located Euler deconvolution solutions (Fig. 5a-d) imply thin sedimentary cover at the central part of the PRB. The solutions based on SI values of 2 and 3 suggest thick sedimentary successions beyond 2 km and 2.5 km in the southern and northern parts of the basin, respectively. With regard to petroleum exploration, areas with thick sedimentary cover are more prospective than areas with thin sedimentary successions (Tiercelin et al., 2004; Abdelazeem et al., 2021).

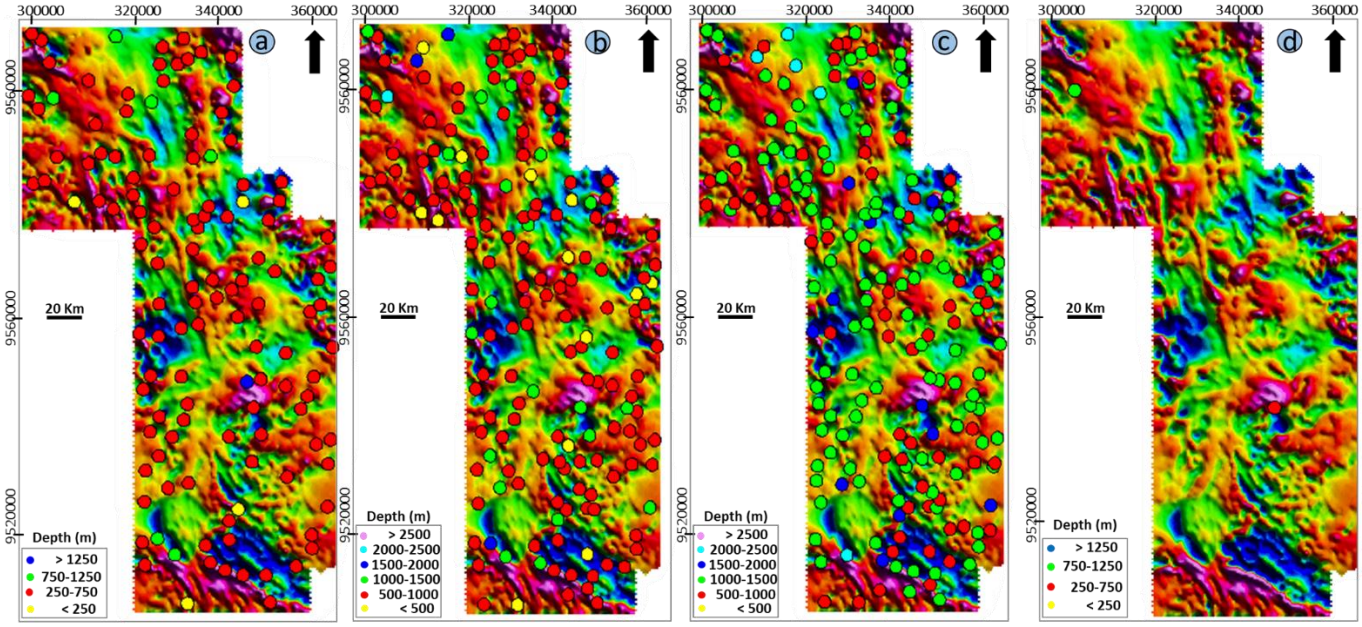


**Figure 5**: Located Euler deconvolution maps of magnetic data computed by using a window size of 20 with a) SI=1 (sill/dike), b) SI=2 (cylinder/pipe), c) SI=3 (sphere), and d) SI=0 (contacts).

**Spectral Depth Analysis**

For depth analysis, the total magnetic intensity map was divided into three blocks (Fig. 4d). These are block A (northern part of the basin), block B (central part of the basin) and block C (southern part of the basin). Thereafter, separation spectrum was produced whereby the estimated depth values are presented in Table 1. Based on radially averaged spectrum, the estimated depths are 0.46 km at the north, 1.33 km at the middle and 1.86 km at the southern parts of the basin (Fig. 6). Here the depth values show that the southern part has thick cover of sediment than other parts of the basin, contrasting the located Euler deconvolution results. This may have been caused by the fact that the spectral depth analysis estimates average depth based on noises and deep and shallow seated sources which may lead to wrong results (Abbass & Mallam, 2013).

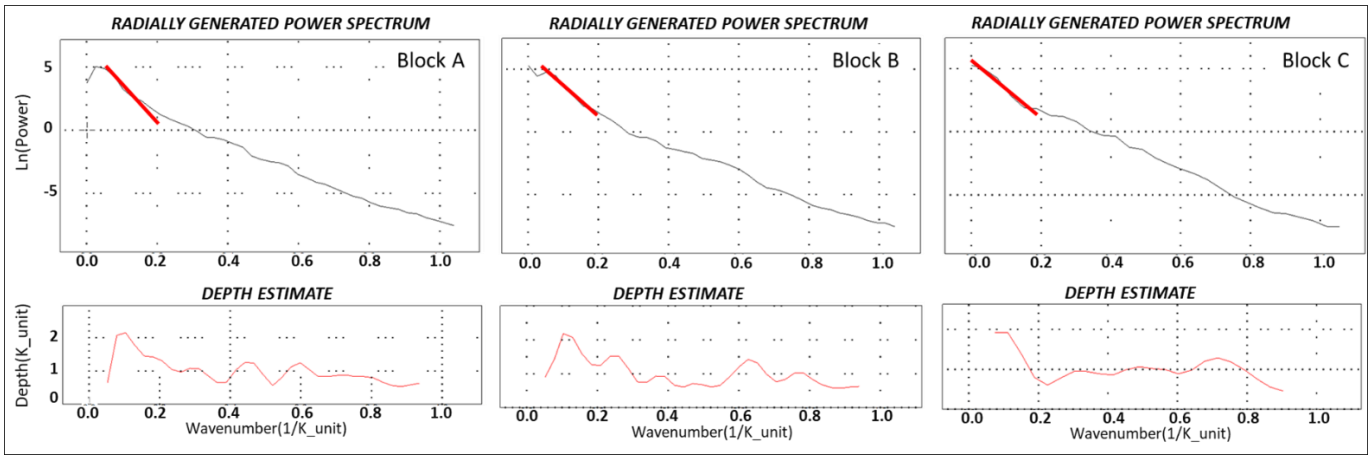


**Figure 6:** Power spectrum graphs of a) Block A, b) Block B, and c) Block C of the study area showing depths to the magnetic sources (red solid line correspond to deep magnetic sources). K_unit = km.

**Table 1:** Average depth to basement for spectral depth analysis of magnetic data.

| Block | A | B | C |
|---|---|---|---|
| Depth (km) | 0.46 | 1.33 | 1.86 |

## Discussion

### Basin Configuration and Sediment Thickness

Interpretation of potential field data allowed establishment of the PRB configuration. This was possible because the used datasets can delineate boundaries of different lithologies (Blaikie et al., 2014). The PRB is narrow and wide at the central and northern and southern parts, respectively. This configuration suggests possible existence of a compartmentalized system where several isolated depocenters may be present. These wide and narrow areas conform to areas with thick and thin sedimentary covers, respectively. This gives a clue of where future petroleum exploration efforts should be focused. The authors of this work recommend further studies in areas with thick sedimentary successions (north and southern parts of the basin).

The located Euler deconvolution solutions estimated maximum sediment thickness to be 2.5 km in the northern part of the PRB (Fig. 5). On the contrary, the spectral depth method estimated relatively thin sedimentary cover (1.86 km) in the same area. Operationally, the spectral depth analysis method is inconsistent especially in fitting a tangent; size of the window tends to vary and sometimes overlap with the grid causing considerable depth underestimation when compared to the Euler deconvolution method. Therefore, the located Euler deconvolution solutions maximum sediment thickness (2.5 km) is considered to be most reliable. The minimum sediment thickness of 2-3 km is needed for most of the rift basin to be considered prospective. This is evident from several discoveries in different parts of the world (Tiercelin et al., 2004; Abdelazeem et al., 2021). In the East African Rift basins for example, the petroleum discoveries have been made in sedimentary basins with maximum sediment thickness ranging from 2 - 4 km (Mutebi et al., 2021). Therefore, the estimated maximum sediment thickness in the PRB (2.5 km) is quite favorable for deposition, preservation, and cooking of organic material for possible petroleum generation.

### Faults and Igneous Intrusions

Lineaments mapping has shown that the PRB is dissected by several faults (Fig. 4c). Major faults have the NNW-SSE

trend conforming to the regional faults trend for the EARS (Foster et al., 1997; Mbede, 2001); minor faults have the N-S and NNE-SSW trends. Different fault trends and orientations imply that the crust experienced different strengths of the tectonic forces during basin development (Ebinger et al., 1997; Foster et al., 1997; Mbede, 2001). These faults can form potential migration pathways for hydrocarbons generated by the deep-seated source intervals to shallow seated reservoirs, if there are any. Additionally, fault systems are known to form potential structural traps in different basins. Thorough knowledge of the structural anatomy of any sedimentary basin is crucial for a petroleum exploration (Harding, 1985; Huang & Liu, 2017). The structural anatomy and timing of occurrence control basin development and migration and trapping of petroleum (Hindle, 1997; Zeng et al., 2010). Therefore, for a full understanding of the petroleum prospectivity of the PRB, further study will focus on detailed structural mapping. This will be achieved by using seismic reflection data with high quality. In the current study, it has also been shown that the igneous intrusions are dominantly increasing toward the north and northwestern parts of the PRB. That is, the concentration of these intrusions is increasing toward the Mountain Kilimanjaro, an area previously considered to be the southernmost limit of the volcanic activities linked to the EARS (Ebinger et al., 1997). The locations of the igneous intrusions are conforming to the locations of the mapped faults (Fig. 4b). This suggests that the mapped faults were the magma conduits, and that tectonic activities played a key role in the evolution of the PRB. Magmatic intrusions have significant impact in the petroleum systems of the associated basins; they can facilitate source rock maturation, form structural traps (including localized intrusion forced folds), and create migration pathways (Planke et al., 2005).

## Conclusion

The current study utilized potential field data (gravity and magnetic) with qualitative and quantitative interpretation approaches to reveal that the PRB contains igneous intrusions that are dominantly increasing toward the north and northwestern parts of the basin. The locations of these intrusions coincide to locations of the mapped faults. This suggests that the mapped faults formed magma conduits and that tectonism had massive influence in basin development. The mapped faults and igneous intrusions may be forming potential petroleum migration pathways and traps (including faults and intrusion forced folds) in the PRB. Our results also show that the PRB contains three major compartments; the north, central and southern compartments. The northern compartment contains thick sedimentary successions (up to 2.5 km thick) sufficient enough to allow source rock maturation, petroleum migration and trapping in the PRB.

## Acknowledgements

The used datasets were provided by Petroleum Upstream Regulatory Authority (PURA). PURA is also appreciated for allowing publication of the results of this work.

## Competing Interest Statement

The authors of this work declare that they have no known conflict of interest or personal relationship and political motives that could have appeared to influence the results of the submitted work.

## Data Availability Statement

The datasets used to support the findings of this study are not publicly available due to confidentiality agreement.

## Authors' Contribution Statement

Ernest Selestin: Conceptualization, interpretation of Potential field datasets, annotation of figures, writing original draft and text editing, visualization, discussion

Emily Barnabas Kiswaka: Potential field data interpretation, annotation of figures, text writing and editing, visualization, supervision

Obeid Saitabau Lemna: Interpretation of Potential field data, text editing, supervision, discussion

Elisante Elisaimon Mshiu: Text review and editing, final manuscript review, supervision, discussion

**References**

Abbass, A. A., & Mallam, A. (2013). Estimating the thickness of sedimentation within Lower Benue Basin and Upper Anambra Basin, Nigeria, using both spectral depth determination and source parameter imaging. International Scholarly Research Notices. https://doi.org/10.1155/2013/124706.

Abdelazeem, M., Fathy, M. S., & Gobashy, M. (2021). Magnetometric Identification of Sub-basins for Hydrocarbon Potentialities in Qattara Ridge, North Western Desert, Egypt. *Pure and Applied Geophysics*. *178*, 995-1020. DOI:10.1007/s00024-021-02678-2.

Bagdasaryan, G. P., Gerasimovskiy, VI., Polyakov, A. I., Gukasyan, R. K., & Vernadskiy, VI. (1973). Age of volcanic rocks in the rift zones of East Africa. *Geochemistry International. 10*, 66-71.

Baker, M. (2012). Landsat interpretation of Pangani Rift (for Swala Energy). Unpublished report.

Blaikie, T. N., Ailleres, L., Betts, P. G., & Cas, R. A. F. (2014). Interpreting subsurface volcanic structures using geologically constrained 3-D gravity inversions: examples of maar-diatremes, Newer Volcanics Province, southeastern Australia. *Journal of Geophysical Research*: *Solid Earth. 119*, 3857-3878. https://doi.org/10.1002/2013JB010751.

Briggs, I. C. (1974). Machine contouring using minimum curvature. Geophysics. *3*, 39-48. http://dx.doi.org/10.1190/1.1440410.

Chorowicz, J. (2005). The East African Rift System. *Journal of African Earth Sciences*. *43*, 379-410. https://doi.org/10.1016/j.jafrearsci.2005.07.019.

Dentith, M., & Cowan, D. (2011). Using potential field data for petroleum exploration targeting, Amadeus Basin, Australia. *Exploration Geophysics*. *42*, 190-198. https://doi.org/10.1071/EG10018.

Corry, C. E. (1988). Laccoliths: mechanism of emplacement and growth. Vol. 220, *Geological Society of America*.

Ebinger, C., Djomani, Y. P., Mbede, E., Foster, A., & Dawson, J. B. (1997). Rifting archaean lithosphere: the Eyasi-Manyara-Natron rifts, East Africa. *Journal of the Geological Society. 154*, 947-960. https://doi.org/10.1144/gsjgs.154.6.0947.

Foster, A., Ebinger, C., Mbede, E., & Rex, D. (1997). Tectonic development of the northern Tanzanian?? sector of the East African Rift System. *Journal of the Geological Society. 154*, 689-700. https://doi.org/10.1144/gsjgs.154.4.0689.

Ferdinand, R. W. (2021). Probabilistic seismic hazard assessment and site analyses of Arusha International Conference Centre (AICC), Arusha, Tanzania. *Tanzania Journal of Science*. *47*, 826-840. DOI:10.4314/tjs.v47i2.37.

Franke, D., Jokat, W., Ladage, S., Stollhofen, H., Klimke, J., Lutz, R., Mahanjane, E. S., Ehrhardt, A., & Schreckenberger, B. (2015). The offshore East African Rift System: Structural framework at the toe of a juvenile rift. *Tectonics*. *34*, 2086-2104. https://doi.org/10.1002/2015TC003922.

Ganiyu, S. A., Badmus, B. S., Awoyemi, M. O., Akinyemi, O. D., & Olurin, O.T. (2013). Upward continuation and reduction to pole process on aeromagnetic data of Ibadan Area, South-Western Nigeria. *Earth Science Research*. 2: p.66. DOI:10.5539/esr.v2n1p66.

Harding, T. P. (1985). Seismic characteristics and identification of negative flower structures, positive flower structures, and positive structural inversion. *AAPG bulletin*. *69*, 582-600. https://doi.org/10.1306/AD462538-16F7-11D7-8645000102C1865D.

Hindle, A. D. (1997). Petroleum Migration Pathways and Charge Concentration: A Three-Dimensional Model. *AAPG Bulletin. 81*, 1451–1481. doi: https://doi.org/10.1306/3B05BB1E-172A-11D7-8645000102C1865D.

Huang, L., & Liu, C. Y. (2017). Three types of flower structures in a divergent-wrench fault zone. Journal of Geophysical Research: Solid Earth. *122*, 10-478. DOI:10.1002/2017JB014675.

Le Gall, B., Nonnotte, P., Rolet, J., Benoit, M., Guillou, H., Mousseau-Nonnotte, M., Albaric, J., & Déverchère, J. (2008). Rift propagation at craton margin. Distribution

of faulting and volcanism in the North Tanzanian Divergence (East Africa) during Neogene times. Tectonophysics. 448: 1-19. https://doi.org/10.1016/j.tecto.2007.11.005.

Lemna, O. S., Stephenson, R., & Cornwell, D. G. (2019). The role of pre-existing Precambrian structures in the development of Rukwa Rift Basin, southwest Tanzania. *Journal of African Earth Sciences*. 150, 607-625. https://doi.org/10.1016/j.jafrearsci.2018.09.015.

Macgregor, D. (2015). History of the development of the East African Rift System: A series of interpreted maps through time. *Journal of African Earth Sciences*. *101*, 232-252. https://doi.org/10.1016/j.jafrearsci.2014.09.016.

Macheyeki, A. S., Delvaux, D., De Batist, M., & Mruma, A. (2008). Fault kinematics and tectonic stress in the seismically active Manyara–Dodoma Rift segment in Central Tanzania–Implications for the East African Rift. *Journal of African Earth Sciences*. *51*,163-188. https://doi.org/10.1016/j.jafrearsci.2008.01.007.

Mollel, G. F., & Swisher III, C. C. (2012). The Ngorongoro Volcanic Highland and its relationships to volcanic deposits at Olduvai Gorge and East African Rift volcanism. *Journal of human evolution*. *63*, 274-283. https://doi.org/10.1016/j.jhevol.2011.09.001.

Monreal, F. R., Villar, H. J., Baudino, R., Delpino, D., & Zencich, S. (2009). Modeling an atypical petroleum system: A case study of hydrocarbon generation, migration and accumulation related to igneous intrusions in the Neuquen Basin, Argentina. *Marine and Petroleum Geology*. *26*, 590-605. https://doi.org/10.1016/j.marpetgeo.2009.01.005.

Mutebi, S., Sen, S., Sserubiri, T., Rudra, A., Ganguli, S.S., & Radwan, A. E. (2021). Geological characterization of the Miocene–Pliocene succession in the Semliki Basin, Uganda: Implications for hydrocarbon exploration and drilling in the East African Rift System. *Natural Resources Research*. *30*, 4329-4354. DOI:10.1007/s11053-021-09951-0.

Mbede, E. I. (2001). Tectonic setting and uplift analysis of the Pangani rift basin in northern Tanzania using apatite fission track thermochronology. Tanzania Journal of Science. 27: 23-38. DOI: 10.4314/tjs.v27i2.18344.

McConnell, R. B. (1972). Geological development of the rift system of Eastern Africa. *Geological Society of America Bulletin*. *83*, 2549-2572. https://doi.org/10.1130/0016-7606(1972)83[2549:GDOTRS]2.0.CO;2.

Nabighian, M. N., Grauch, V. J. S., Hansen, R. O., LaFehr, T. R., Li, Y., Peirce, J. W., Phillips, J. D., & Ruder, M. E. (2005). The historical development of the magnetic method in exploration. *Geophysics 70*, 33-61. https://doi.org/10.1190/1.2133784.

Planke, S., Rasmussen, T., Rey, S. S., & Myklebust, R. (2005). Seismic characteristics and distribution of volcanic intrusions and hydrothermal vent complexes in the Vøring and Møre basins. In *Geological Society, London, Petroleum Geology Conference series. 6*, 833-844. https://doi.org/10.1144/0060833.

Rajaram, M. (2006). Utilizing Magnetic Signatures Related to Hydrocarbons. In *6th International Conference & Exposition on Petroleum Geophysics.* 63-65.

Reid, A. B., Allsop, J. M., Granser, H., Millett, A.T., & Somerton, I. W. (1990). Magnetic interpretation in three dimensions using Euler deconvolution. *Geophysics*, *55*(1), 80-91. https://doi.org/10.1190/1.1442774.

Ring, U. (2014). The East African rift system. *Austrian J. Earth Sci. 107*, 132-146.

Telford, W. M., Geldart, L. P., & Sheriff, R. E. (1990). Applied geophysics. Cambridge University Press. https://doi.org/10.1017/CBO9781139167932,

Tiercelin, J. J., Potdevin, J. L., Morley, C. K., Talbot, M. R., Bellon, H., Rio, A., Le Gall, B., & Vétel, W. (2004). Hydrocarbon potential of the Meso-Cenozoic Turkana Depression, northern Kenya. I. Reservoirs: Depositional environments, diagenetic characteristics, and source rock–reservoir relationships. *Marine and Petroleum Geology*. *21*, 41-62.

Thompson, D. T. (1982). EULDPH: A new technique for making computer-assisted depth estimates from magnetic data. *Geophysics*. *47*, 31-37. https://doi.org/10.1190/1.1441278.

Uieda, L., Oliveira Jr, V. C., & Barbosa, V. C. (2014). Geophysical tutorial: Euler deconvolution of potential-field data. *The Leading Edge*. *33*, 448-50. https://doi.org/10.1190/tle33040448.1.

Verduzco, B., Fairhead, J. D., Green, C. M., & MacKenzie, C. (2004). New insights into magnetic derivatives for structural mapping. *The Leading Edge*. *23*, 116-119. https://doi.org/10.1190/1.1651454.

Witte, J., Trümpy, D., & Babies, H. G. (2016). The Role of Neo-Tectonics in Oil Migration, Lake Turkana Region, Kenya. In SPE/AAPG Africa Energy and Technology Conference. OnePetro.

Zeng, L., Wang, H., Gong, L., & Liu, B. (2010). Impacts of the tectonic stress field on natural gas migration and accumulation: A case study of the Kuqa Depression in the Tarim Basin, China. *Marine and Petroleum Geology*. *27*, 1616-1627. DOI:10.1016/j.marpetgeo.2010.04.010.